⌘ *Author's Choice*

THE JOURNAL OF BIOLOGICAL CHEMISTRY VOL. 287, NO. 45, pp. 38124–38134, November 2, 2012

Vascular Bioactivation of Nitroglycerin by Aldehyde Dehydrogenase-2

REACTION INTERMEDIATES REVEALED BY CRYSTALLOGRAPHY AND MASS SPECTROMETRY[*] [S]

Received for publication, April 12, 2012, and in revised form, September 14, 2012 Published, JBC Papers in Press, September 17, 2012, DOI 10.1074/jbc.M112.371716

Barbara S. Lang[‡], Antonius C. F. Gorren[‡], Gustav Oberdorfer[§], M. Verena Wenzl[‡], Cristina M. Furdui[¶], Leslie B. Poole[‖], Bernd Mayer[‡1], and Karl Gruber[§2]

From the [‡]Department of Pharmacology and Toxicology and the [§]Institute of Molecular Biosciences, University of Graz, 8010 Graz, Austria, and the Departments of [¶]Internal Medicine and [‖]Biochemistry, Wake Forest School of Medicine, Winston-Salem, North Carolina 27157

Background: Aldehyde dehydrogenase-2 (ALDH2) catalyzes bioactivation of glyceryl trinitrate (GTN) resulting in vasodilation. The exact mechanism is still unclear.
Results: Structures of ALDH2 in complex with GTN and of a thionitrate intermediate were obtained.
Conclusion: The structures represent snapshots of the first reaction step of GTN bioactivation by ALDH2.
Significance: The results provide new insight into the mechanism of vascular GTN bioactivation by ALDH2.

Aldehyde dehydrogenase-2 (ALDH2) catalyzes the bioactivation of nitroglycerin (glyceryl trinitrate, GTN) in blood vessels, resulting in vasodilation by nitric oxide (NO) or a related species. Because the mechanism of this reaction is still unclear we determined the three-dimensional structures of wild-type (WT) ALDH2 and of a triple mutant of the protein that exhibits low denitration activity (E268Q/C301S/C303S) in complex with GTN. The structure of the triple mutant showed that GTN binds to the active site via polar contacts to the oxyanion hole and to residues 268 and 301 as well as by van der Waals interactions to hydrophobic residues of the catalytic pocket. The structure of the GTN-soaked wild-type protein revealed a thionitrate adduct to Cys-302 as the first reaction intermediate, which was also found by mass spectrometry (MS) experiments. In addition, the MS data identified sulfinic acid as the irreversibly inactivated enzyme species. Assuming that the structures of the triple mutant and wild-type ALDH2 reflect binding of GTN to the catalytic site and the first reaction step, respectively, superposition of the two structures indicates that denitration of GTN is initiated by nucleophilic attack of Cys-302 at one of the terminal nitrate groups, resulting in formation of the observed thionitrate intermediate and release of 1,2-glyceryl dinitrate. Our results shed light on the molecular mechanism of the GTN denitration reaction and provide useful information on the structural requirements for high affinity binding of organic nitrates to the catalytic site of ALDH2.

Nitroglycerin (glyceryl trinitrate, GTN)[3] was first synthesized in the nineteenth century when searching for new, highly potent explosives and has been successfully used for the treatment of angina pectoris and congestive heart failure for more than 100 years (1). GTN belongs to the group of organic nitrates that cause vasodilation via nitric oxide (NO)-mediated activation of soluble guanylate cyclase. The clinical use of GTN is limited by a loss of efficacy upon continuous application, a phenomenon referred to as vascular nitrate tolerance (2, 3).

There is large body of evidence that the bioactivation of GTN is mediated by aldehyde dehydrogenase-2 (ALDH2) (4). Aldehyde dehydrogenases are NAD(P)-dependent oxidoreductases that detoxify aldehydes through oxidation to the corresponding acids (5) and can be found in animals, fungi, and bacteria (6). Mature human ALDH2 has 500 amino acids and a molecular mass of ~54 kDa. It is expressed in tissues of liver, kidney, heart, lung, and brain (7) and is involved in detoxification of ethanol through the conversion of acetaldehyde to acetic acid (8). About 40% of the East Asian population have an inactive mutant of the enzyme leading to impaired alcohol tolerance, which is accompanied by a decreased risk for alcoholism (9). Besides, this mutation is also associated with an increased risk for various cancers, alcoholic liver disease, and cirrhosis (7, 10, 11).

In addition to the dehydrogenase reaction, ALDH2 also exhibits esterase (12) and the aforementioned denitration activity (13). In 2002, Stamler and co-workers (13) showed that the enzyme converts GTN to 1,2-GDN and nitrite. They reasoned that GTN denitration may resemble esterase activity in a way that the substrate undergoes nucleophilic attack by the active site Cys-302. Thus, a thionitrate would be formed, which

* This work was supported, in whole or in part, by National Institutes of Health Grant R01 GM050389 (to L. B. P.) and the Austrian Science Fund (FWF) through Project Grants P20669 and P21693 (to B. M.) and P19858 (to K. G.) and through the Ph.D. program "Molecular Enzymology" W901 (to B. M. and K. G.).
⌘ *Author's Choice*—Final version full access.
[S] This article contains supplemental Table S1 and Figs. S1–S3.
[1] To whom correspondence may be addressed: University of Graz, Universitätsplatz 2, 8010 Graz, Austria. Tel.: 43-316-380-5567; Fax: 43-316-380-9890; E-mail: mayer@uni-graz.at.
[2] To whom correspondence may be addressed: Institute of Molecular Biosciences, University of Graz, Humboldtstraße 50/3, 8010 Graz, Austria. Tel.: 43-316380-5483; Fax: 43-316380-9897; E-mail: karl.gruber@uni-graz.at.

[3] The abbreviations used are: GTN, glyceryl trinitrate; ALDH2, aldehyde dehydrogenase-2 (EC 1.2.1.3); GDN, glyceryl dinitrate; DTT, dithiothreitol; TCEP, tris(2-carboxyethyl)phosphine; BisTris, bis(2-hydroxyethyl)imininotris(hydroxymethyl)methane; ADP, atomic displacement parameters; DTPA, diethylenetriaminepentaacetic acid; ESI-TOF MS, electrospray ionization-time of flight mass spectrometry.

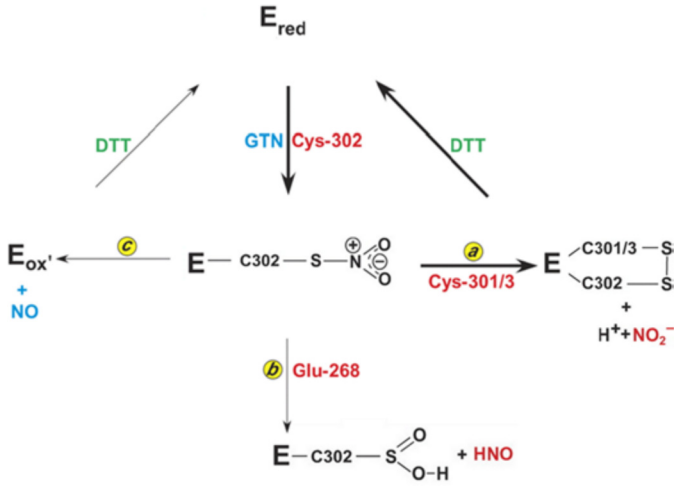

SCHEME 1. **Proposed reaction mechanism of GTN denitration modified from Ref. 16.** After nucleophilic attack of Cys-302 on the first nitrate group of GTN, a thionitrate, the central intermediate, is formed. The major reaction pathway (*a*), in which Cys-301 and Cys-303 are involved, results in the formation of nitrite and an oxidized enzyme, presumably a species with a disulfide bond in the active site, which can be regenerated by reductants like DTT. *b,* depicts the pathway yielding an irreversibly inactivated enzyme, possibly due to oxidation of Cys-302 to a sulfinic acid. For this pathway Glu-268 is essential. *c,* leads to a reversibly inhibited enzyme and the production of NO.

in turn would be attacked by one of the two flanking cysteine residues (301 or 303) to form a disulfide bond. Nitrite would be released and further reduced to NO (13). However, our group found that a fraction of 5–10% of GTN is directly reduced to NO, which may be sufficient for ALDH2-mediated bioactivation in blood vessels (14, 15).

Wenzl *et al.* (16) proposed three different pathways for the denitration reaction (Scheme 1). All of them have the first reaction step in common, which is the formation of the thionitrate and the release of 1,2-GDN. The proposed main reaction pathway resembles the mechanism initially suggested by Stamler and co-workers (13) and results in an inhibited enzyme that can be reactivated by certain reducing agents such as dithiothreitol (DTT). The second pathway potentially leads to an irreversibly inactivated enzyme, presumably mediated by Glu-268, whereas only the third pathway yields NO (16). Irreversible enzyme inactivation as described in the second pathway (Scheme 1) is thought to be a major factor in the development of nitrate tolerance (17).

In our study we soaked crystals of ALDH2 (wild-type (WT) and the E268Q/C301S/C303S mutant) with GTN and determined the structures to 2.3- and 2.2-Å resolution, respectively. In crystals of the ALDH2 triple mutant we observed GTN bound in the active site in close proximity to Cys-302, whereas crystals of the wild-type enzyme contained the thionitrate intermediate common to all proposed reaction pathways. A thionitrate adduct was also observed by mass spectrometry of ALDH2 treated with GTN in solution, strengthening the evidence that it is indeed a central intermediate.

Thus, the two structures can be seen as snapshots of the first reaction step of the bioactivation of GTN, *i.e.* the formation of the thionitrate through the nucleophilic attack of Cys-302 on GTN. Analysis of the structures also revealed residues important for binding of GTN and provided information on the properties of organic nitrates required for bioactivation by ALDH2.

EXPERIMENTAL PROCEDURES

Materials—Sephacryl S-300 HR was purchased from GE Healthcare Europe GmbH. Resource Q column (6 ml) was obtained from Pharmacia Biotech. Pierce unstained molecular mass markers (14.4–116.0 kDa) for SDS-PAGE were from Thermo Scientific. [2-^{14}C]GTN (50–60 mCi/mmol) was from American Radiolabeled Compounds, purchased through Hartmann Analytics GmbH (Braunschweig, Germany). Nitropohl ampoules (G. Pohl-Boskamp GmbH and Co., Hohenlockstedt Germany), containing 4.4 mM GTN in 250 mM glucose, were obtained from a local pharmacy. 1,2-GDN, 1,3-GDN, and GTN, used as standards in radio-thin layer chromatography, were purchased from LGC Promochem (Wesel, Germany). Tris(2-carboxyethyl)phosphine (TCEP) hydrochloride was obtained from Biosynth AG (Staad, Switzerland). CrystalClear strips were obtained from Douglas Instruments Ltd.

Professor Wing-Ming Keung (Harvard Medical School) and Professor Andreas Daiber (Medical Center of Johannes Gutenberg University, Germany) kindly provided daidzin and a 450 mM GTN solution in ethanol, respectively. All other chemicals were purchased from Sigma.

Site-directed Mutagenesis—E268Q/C301S/C303S mutations were inserted using the QuikChange II site-directed mutagenesis kit (Stratagene, Heidelberg, Germany). To introduce the mutation (bold type) and to add the BamHI restriction site (underlined) as a silent mutation for screening of mutants to the cDNA encoding for WT ALDH2, the following mutagenic sense primers were used: 5′-GTT CTT CAA CCA GGG CCA G**TC C**TG C**TC T**GC CGG aTC CCG GAC CTT CGT G-3′ for C301S/C303S. To introduce the E268Q mutation (bold type) and to add the AflII restriction site (underlined) as a silent mutation for screening of mutants to the cDNA encoding for C301S/C303S-ALDH2, the mutagenic sense primer 5′-GCA GCA ACC TtA AG-A GAG TGA CCT TG**C AG**C TGG GGG GGA AG-3′ was used. Sequencing of cDNAs was performed with an ABI 373A automated DNA sequencer (Applied Biosystems, Carlsbad, CA) to confirm the desired mutations.

Protein Purification—Human ALDH2 was expressed in *Escherichia coli* BL21(DE3) and purified by affinity and size exclusion chromatography as described (14, 18). Because protein samples from initial purification trials did not yield crystals using the published conditions (19–25) we further purified the protein by ion exchange chromatography as described for horse liver ALDH2 (26) in addition to optimizing the crystallization conditions. The enzyme eluted from the size exclusion column was diluted into a 20 mM 2-amino-2-(hydroxymethyl)-1,3-propanediol hydrochloride (Tris-HCl) buffer containing 50 mM sodium chloride and 200 μM DTT (low salt buffer). This solution was applied to a Resource Q column (equilibrated with low salt buffer), washed with 30 ml of low salt buffer, and eluted using a gradient of high salt buffer (20 mM Tris-HCl, 1 M sodium chloride, and 200 μM DTT).

An SDS-PAGE gel was made with those fractions that gave an absorption peak at 280 nm. Fractions that had a band at ~50 kDa were pooled and dialyzed against 100 mM MES buffer containing 200 μM $MgCl_2$. The dialyzed enzyme was concentrated

to ~4 mg/ml and stored at −20 °C. An SDS-PAGE gel of the purified enzyme is provided as supplemental Fig. S1.

First crystallization experiments (see below) were done in parallel with enzyme batches purified with the conventional purification method as well as with batches purified with the additional ion exchange chromatography step. The best diffracting crystals of the wild-type enzyme were produced from protein that was further purified using ion exchange chromatography. However, subsequent experiments showed that this additional purification step was not absolutely necessary for crystallization. Therefore, the additional step was dropped from the purification of the ALDH2 mutant E268Q/C301S/C303S.

Crystallization—For crystallization the triple mutant and the wild-type enzyme were used. Crystals were obtained using the vapor diffusion sitting drop method at 20 °C from solutions containing ~5 (triple mutant) or ~3 mg/ml (wild-type) enzyme. The following compounds were added to these solutions at the given final concentrations: 6.9 mM $MgCl_2$, 4.6 mM TCEP, 2.3 mM NAD^+, and 47.6 mM glucose were added to the triple mutant and 13.3 mM $MgCl_2$, 8.9 mM TCEP, 4.4 mM NAD^+, and 45.8 mM glucose were added to the wild-type. These solutions were equilibrated for 4 h at room temperature before mixing them with an equal volume (1 μl) of reservoir solution consisting of 100 mM BisTris, pH 6.4, 25% PEG 3350, and 60 mM urea. After about 16 h the drops were streak-seeded and crystals were harvested after 9 to 10 days.

Soaking—For the soaking of wild-type crystals 0.5 μl of 4.4 mM GTN solution were added to the drop. After 3 min an additional 0.5 μl of GTN solution were pipetted onto the drop so that the final GTN concentration was about 1.5 mM. The crystal was harvested immediately afterward and flash-cooled in liquid nitrogen.

Crystals of the triple mutant were soaked using a different approach. Crystals were transferred to a new drop differing from the original one only in that it additionally contained 0.2 μl of a 450 mM GTN solution, which gives an estimated GTN concentration of about 41 mM. The crystals were left in this solution for about 10 min before they were mounted and flash-cooled.

Data Collection and Structure Determination—Diffraction data were collected at the European Synchrotron Radiation Facility (ESRF), beamline ID 14-4 (27), and at the Deutsche Elektronen-Synchrotron (DESY), beamline X13. These data were indexed and integrated using the XDS package (28) and scaled using the program Scala (29).

ALDH2 crystals are known to crystallize either in space groups $P2_12_12_1$ or $C222_1$ (19). The C-centered orthorhombic ALDH2 crystals often suffer from pseudomerohedral twinning and diffraction data had to be processed in $P2_1$. However, the dataset obtained from our WT crystal could be processed in the $C222_1$ without any indication of twinning. In contrast, data for the triple mutant had to be processed in $P2_1$ and showed clear signs of pseudomerohedral twinning with a (refined) twin fraction of 0.21 and a twin law of *l,-k,h*. Therefore, the selection of reflections for the calculation of R_{free} took the twin law into account (30).

The structures were solved by molecular replacement using the program Phaser (31). A sole monomer of the human ALDH2 wild-type structure served as the search model (19, 23).

Refinement was done with the programs Phenix (version 1.7.3) (30) and Coot (32). The weights of the x-ray target relative to stereochemical and ADP restraints were optimized during last rounds of refinement.

After several rounds of refinement of the triple mutant structure, difference electron density appeared in one of eight chains in the asymmetric unit, which could not be explained by water. Using the program Phenix LigandFit (33, 34) this density was interpreted as GTN bound in the active site (supplemental Fig. S2). Its occupancy was refined to 0.58 in the final model. The R_{work} and R_{free} factors were 13.2 and 16.7%, respectively.

Initial refinement of the wild-type structure revealed a density blob in the $F_o - F_c$ map as well as the $2F_o - F_c$ map at the sulfur atom of Cys-302, which could best be fitted by a thionitrate (supplemental Fig. S3). In this case, the thionitrate is found in all four chains of the asymmetric unit. The occupancy of the adduct was refined and converged at values from 0.86 to 0.97 in the final structure. Final *R*-values were 17.0 and 20.9% (R_{free}).

Geometric restraints for GTN and the thionitrate adduct were generated using the PRODRG server (35) and were adjusted according to the Cambridge Structural Database entries CORYIR10 (36) and VIQDUU (37), respectively. A detailed description of the data collection, processing, and refinement statistics can be found in supplemental Table S1.

Mass Spectrometry—Wild-type and the triple mutant of ALDH2 (126 and 130 μM, respectively) were preincubated with 1 mM NAD, 0.1 mM diethylenetriaminepentaacetic acid (DTPA), and 3 mM $MgCl_2$ in 50 mM phosphate buffer, pH 7.4. Aliquots of 30 μl were then incubated with 100 μM GTN at 25 °C for 10 min. The reaction was stopped by loading the reaction mixture on a BioGel P6 spin column equilibrated with 0.003% formic acid in water. Electrospray ionization-time of flight mass spectrometry (ESI-TOF MS) analysis was performed on an Agilent MSD TOF system in positive ion mode with the following settings: capillary voltage (VCap) 3500 V, nebulizer gas 30 psig (~3.1 bar), drying gas 5.0 liter min^{-1}; fragmentor 140 V; gas temperature 325 °C. The samples were injected at a flow rate of 20 μl min^{-1}, using a syringe pump (KD Scientific). The averaged MS spectra were deconvoluted using Agilent MassHunter Work station software version B.01.03.

Determination of GTN Denitration Activity—The rates of GTN conversion to 1,2- and 1,3-GDN were determined according to a protocol described previously (38). Wild-type ALDH2 protein (4 μg) was incubated with 4 μM ^{14}C-labeled GTN and 6 μM unlabeled GTN or 6 μM ^{14}C-labeled GTN and 94 μM unlabeled GTN, respectively, at 37 °C for 1 min in a final volume of 0.2 ml of 50 mM potassium phosphate buffer, pH 7.4, containing 3 mM $MgCl_2$, 1 mM NAD^+, 1 mM DTT, 0.1 mM DTPA, and 1% dimethyl sulfoxide (DMSO). Daidzin was added to the reaction mixture at final concentrations of 10, 30, 100, 300 μM, and 1 and 10 mM. Reaction products were extracted twice with 1 ml of diethyl ether and separated by thin-layer chromatography. Quantification was done by liquid scintillation counting. Blank values were determined in the absence of protein under identical conditions (with and without 100 μM daidzin) and sub-

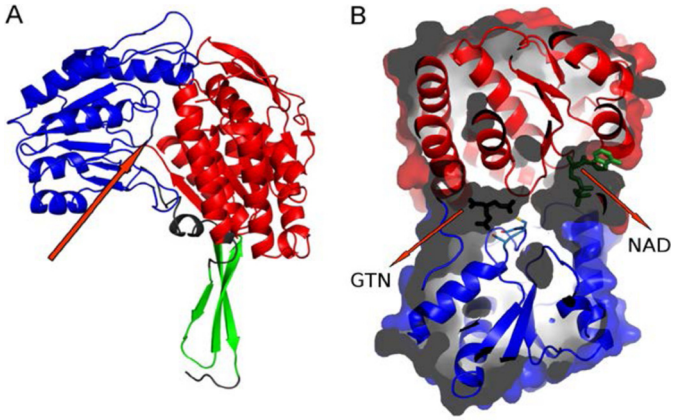

FIGURE 1. **Structure of the triple mutant of ALDH2 in complex with GTN and NAD(H).** *A*, the cofactor binding domain is colored *red*, the catalytic domain *blue*, and the oligomerization domain *green*. One ALDH2 chain is shown. The *arrow* indicates the position of the active site. *B*, surface representation highlighting the cofactor binding site and the active site of ALDH2. GTN is shown in *black* and the cofactor in *green*. Active site residues (Ser-301, Cys-302, and Ser-303) are shown as sticks.

tracted. The results are mean ± S.E. determined in three independent experiments. The rates of 1,3-GDN formation were negligible and are not shown. Assuming competitive inhibition by daidzin, the results were fitted to Equation 1.

$$v = \frac{V_{max} \cdot [S]}{[S] + K_m(1 + [I]/K_i)} \quad \text{(Eq. 1)}$$

At any given GTN concentration of [S] there is an infinite number of the parameters, V_{max}, K_m, and, K_i, that might fit the observations, but there can only be one combination of parameters that will fit the results at both substrate concentrations (10 and 100 μM) simultaneously. We therefore determined values for V_{max} and K_i for a range of pre-set K_m values to determine whether there was such a combination. We obtained virtually identical values for V_{max} and K_i at 10 and 100 μM GTN with a K_m of 8.7 μM (see text).

RESULTS

Overall Structure of ALDH2—We have determined the structure of the ALDH2 triple mutant (E268Q/C301S/C303S) in complex with GTN to a 2.2-Å resolution as well as of the wild-type enzyme with a covalent thionitrate adduct at the catalytically competent Cys-302 to a 2.3-Å resolution. Details of the data collection and processing as well as refinement statistics can be found in supplemental Table S1.

The crystal of the triple mutant contained eight independent protein chains forming two tetramers, whereas the crystal of the wild-type enzyme contained four chains again forming a tetramer. All subunits were virtually identical (with average Cα root mean square deviation values of less than 0.2 Å) and consisted of three domains: the catalytic, the cofactor binding, and the oligomerization domain (Fig. 1*A*).

Formation of a homotetramer is generally observed for ALDH2 (25). In addition, superposition of each subunit with subunit A of the apo wild-type enzyme (PDB code 1o05) revealed average root mean square deviation values of about 0.2 Å, pointing at the overall high similarity between our and published ALDH2 structures.

The catalytic pocket is situated between the catalytic and the cofactor binding domain and expands toward the key active site residue Cys-302 (25) (Fig. 1*B*), which is flanked by two cysteines, Cys-301 and Cys-303. According to a recent publication (16) these are involved in reversible enzyme inhibition, presumably through the formation of a disulfide bond with Cys-302. Glu-268, on the other hand, has been proposed to be a major player in irreversible enzyme inactivation (15, 16). The triple mutant exhibits reduced activity and slower irreversible inactivation. Unlike the wild-type it almost exclusively produces 1,2-GDN and NO (16).

The NAD binding site is located next to the catalytic pocket, on the opposite site of Cys-302 (Fig. 1*B*). NAD(H) is bound by a domain showing a variation of the Rossman-fold (39). In contrast to NAD(H) binding to a typical Rossman-fold, the diphosphate linkage of the cofactor is more flexible in this case (22) with the consequence that the nicotinamide moiety can occur in different, alternate conformations (40). Two of those have been observed in ALDH2 crystal structures. They are called the "hydrolysis" and "hydride transfer" conformation (22). In the latter the cofactor extends into the catalytic pocket and is ready to accept a hydride ion during aldehyde oxidation, whereas it is more contracted in the hydrolysis conformation, allowing product dissociation (22).

Structure of the Triple Mutant in Complex with GTN—During the refinement of the structure of the triple mutant, clear residual electron density was observed in the active site of one of the eight independent chains. This density was best fitted by a molecule of GTN bound to the enzyme with a final, refined occupancy of 0.58. GTN interacts with the side chain of Asn-169 and the main chain amide group of Cys-302 (Fig. 2*A*), which are part of the so-called "oxyanion hole" (41). The O1 atom of the *pro*-S nitrate group is 3.1 Å away from the main chain nitrogen of Cys-302 and 3.6 Å from the side chain of Asn-169. Additionally, O2 of the same group is within 2.9 Å of the side chain of Gln-268 (Fig. 2*A*).

The *pro*-R nitrate group of GTN is bound to the enzyme via polar contacts to the side chain of Ser-301 and through a hydrogen bond to an ordered water molecule (Fig. 2*A*). This water in turn is hydrogen bonded to Asp-457, which also exhibits polar contacts to Ser-303. Ser-303 does not participate in substrate binding in any other way. In addition to these polar contacts, the bound GTN molecule is surrounded by mostly hydrophobic residues: Phe-170, Leu-173, Met-174, Trp-177, Phe-296, Phe-459, and Phe-465. Superposition of the active site of the triple mutant with the active site of the wild-type enzyme shows that neither these mutations nor binding of GTN induce gross conformational changes (Fig. 2*B*).

The side chain of Cys-302 has previously been shown to adopt two different conformations (19–25, 42–46), which are both also observed in the active site of the triple mutant in complex with GTN. One is called the "resting" and the other the "attacking" conformation (47). The resting conformation points away from the substrate (and in the direction of the cofactor in the hydrolysis conformation). In the present structure the resting conformation has a χ1 torsion angle of −58°, whereas this angle is 68° in the attacking conformation. This is

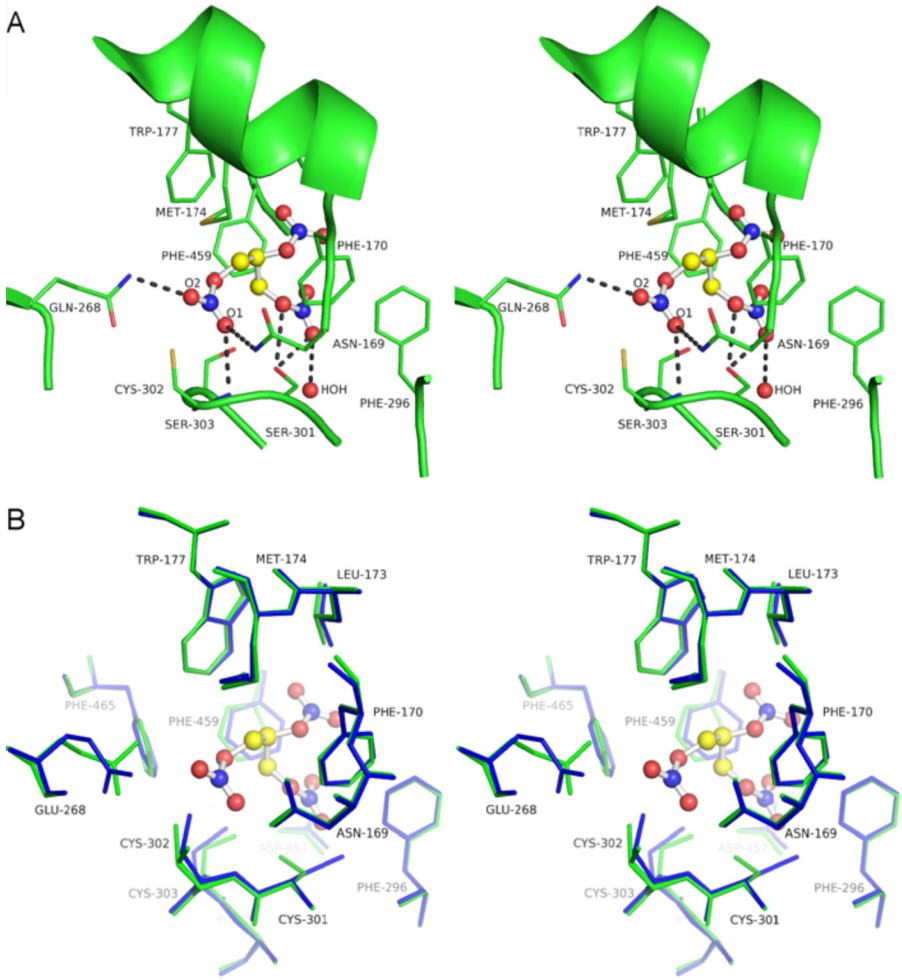

FIGURE 2. **Stereoscopic representation of the complex of the ALDH2 triple mutant with GTN.** *A*, GTN (*yellow*) is shown in a *ball and stick* representation. Active site residues are shown as *sticks*. The resting conformation of Cys-302 has been omitted for clarity. *Dashed lines* indicate polar interactions. *B,* superposition of the active site of the triple mutant (*green*) with that of the apo wild-type enzyme (*blue*, PDB 1o05). Labels refer to the wild-type.

in good agreement with previously published ALDH2 structures (19–25, 48).

Three different conformations of the side chain of Glu-268 have so far been observed in crystal structures of ALDH2 (19–25, 48). They were called the "inside," "intermediate," and "outside" conformation (47). The "outside" conformation is predominantly observed in the "Asian" mutant and is suggested to be the most transitory conformation (48, 49). In contrast, the other two conformations were both observed in the apo wild-type structure with a slight preference for the intermediate conformation (23). In the intermediate conformation, Glu-268 is about 6 Å away from the catalytic cysteine, whereas it is within hydrogen bonding distance of Cys-302 in the inside conformation.

In the structure of the triple mutant all Gln-268 residues (corresponding to Glu-268 in the wild-type) are in the inside conformation. The side chain carbonyl oxygen is hydrogen-bonded to an ordered water molecule. An additional polar contact is formed between the side chain amide group of Gln-268 and the main chain oxygen of Leu-269. If the carboxamide group is flipped, a hydrogen bond between the amide group and the *pro*-S nitrate of the bound GTN can be established (Fig. 2*A*).

The triple mutant was co-crystallized with NAD (see "Experimental Procedures"). In the structure, the density of the AMP part was well defined, whereas the electron density for the nicotinamide moiety was weak. Accordingly, we have not included the nicotinamide ring in four out of the eight chains in the asymmetric unit. The other four chains also lack clear density for the nicotinamide-ribose and therefore we only included ADP in the model. In all chains the pyrophosphate and the ribose, respectively, are in the hydrolysis conformation. Weak or missing electron density for the nicotinamide part is a feature present in several ALDH2 structures (21, 22, 50).

Structure of the Wild-type Thionitrate Adduct—Soaking of crystals of wild-type ALDH2 with GTN resulted in a covalent modification on Cys-302, which is observed in all four chains of the asymmetric unit. We interpreted this modification as a thionitrate adduct (Fig. 3), which is proposed to be the main intermediate of the denitration reaction (Scheme 1). Refined occupancies of this adduct were found between 0.86 and 0.97. The subsequent analysis focused on chain A, because the electron density was clearest in this chain and no significant differences were observed between the chains.

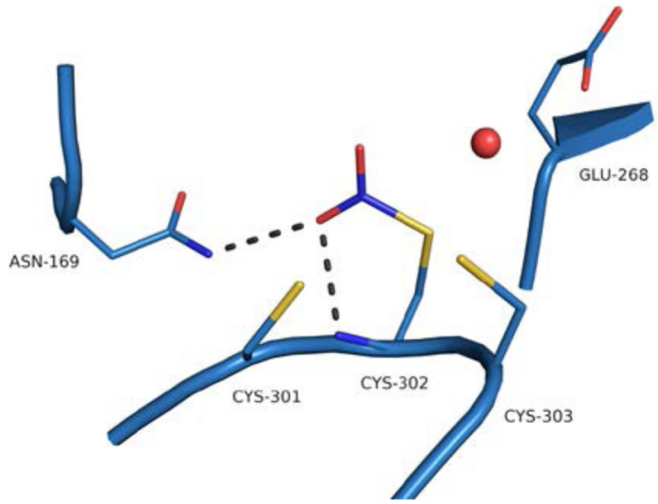

FIGURE 3. **Structure of the thionitrate intermediate as observed in the GTN-soaked WT ALDH2 crystals.** Active site residues as well as the thionitrate adduct are shown as *sticks*. *Dashed lines* indicate polar interactions of the thionitrate. The ordered water molecule is shown as a *red sphere*. The alternate conformation of Cys-301 is not shown for clarity.

Cys-302 is only present in the attacking conformation. The intermediate is stabilized by hydrogen bonds to the side chain amide group of Asn-169 (3.0 Å) and main chain amide of Cys-302 (2.8 Å). Glu-268 is in the intermediate conformation (Fig. 3).

As seen in most ALDH2 structures, the adenine moiety of NAD(H) is well defined, whereas the density for the nicotinamide part is weaker. Increasing flexibility from the adenine to the nicotinamide is also suggested by increasing *B*-factors, which are 14.5 for adenine and ribose, 21.4 for the diphosphate group, and 27.7 for the following ribose and the nicotinamide. Therefore the occupancy of the latter two groups was set to 0.8. In the thus refined structure the cofactor adopts the hydrolysis conformation.

ESI-TOF MS Analysis of the Effect of GTN on WT and the Triple Mutant—To further elucidate the nature of the reaction intermediates, we conducted mass spectrometry experiments. We incubated both the WT and the triple mutant with and without GTN for 10 min under nonreducing conditions (Fig. 4). The calculated mass of the reduced WT (54,431 Da) matched very well the predominant peak at 54,432.26 ± 0.38 Da (from three independent measurements) observed in the WT control experiment.

Assuming equal ionization efficiency of protein and protein-adduct complex as has been shown previously for chymotrypsin (51), the reaction of WT with GTN resulted in three different *m*/*z* species compared with WT control. The most pronounced peak corresponding to a mass of 54,430.74 Da ± 0.20 (around 2/3 of GTN-treated WT) is shifted by −1.52 Da from the reduced enzyme. This shift is statistically significant ($p = 0.004$) and indicates the formation of a disulfide bridge caused by GTN.

The second most prominent enzyme reaction product is shifted +31.4 Da from the reduced enzyme and, notably, distinct from the small apparent impurity present in the enzyme preparation, implying that a fraction of around ⅓ of GTN-treated WT was oxidized to cysteine sulfinic acid at the active

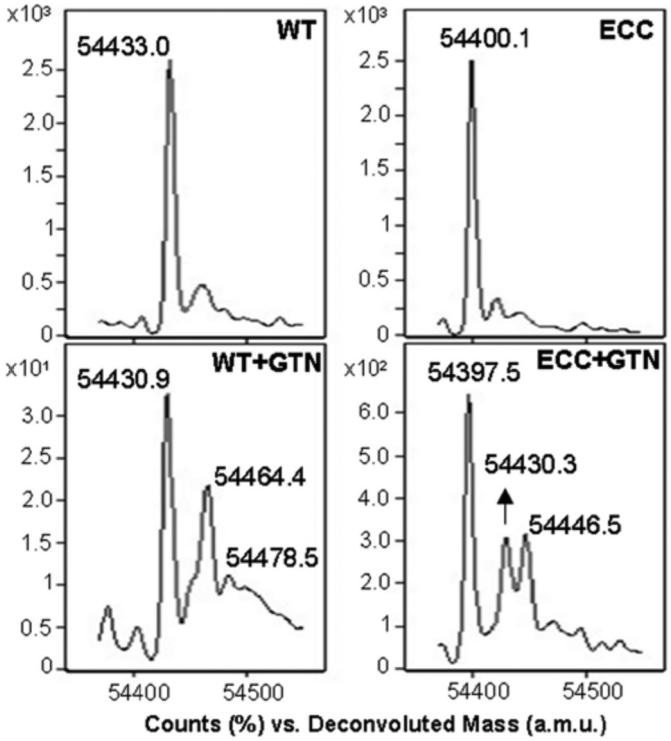

FIGURE 4. **ESI-TOF mass spectrometric analysis of the wild-type (*left panel*) and the triple mutant, abbreviated as ECC (*right panel*).** The enzymes were incubated for 10 min with and without GTN (*lower* and *upper panel*, respectively).

site. The third small but visible peak shifted +45.5 Da away from the reduced enzyme could point to the existence of a thionitrate intermediate. These results correlate reasonably well with the enzyme reaction products proposed in Scheme 1.

Similarly, the triple mutant showed three distinct *m*/*z* species, but with a peak of around 25% of GTN-treated enzyme a more pronounced shift toward the thionitrate intermediate was found (+46.4 Da). Another ~25% of GTN-treated enzyme showed a shift similar to the sulfinic acid peak of GTN-treated WT (+30.2 Da). Evidently, in the case of the triple mutant the *m*/*z* shift of −2.6 cannot be explained by the formation of a disulfide bond. An attractive explanation would be the formation of an intramolecular sulfenamide of the sulfur atom of Cys-302 with the backbone nitrogen of Cys-303 as has been described for protein-tyrosine phosphatases (52–54).

Inhibition of GTN Denitration Activity by Daidzin—The established ALDH2-selective inhibitor daidzin inhibits both aldehyde oxidation and GTN denitration (14, 38). For acetaldehyde dehydrogenation, inhibition was shown to be of the mixed-type with a strong competitive component (55). Comparison of the wild-type-daidzin structure (PDB 2vle) with the triple mutant-GTN structure shows that the binding sites of daidzin and GTN are overlapping (Fig. 5*A*), suggesting that inhibition of denitration is GTN competitive.

As shown in Fig. 5*B*, daidzin inhibited formation of 1,2-GDN from 10 and 100 μM GTN with IC_{50} values of 35 ± 4 and 222 ± 18 μM, respectively, indicating GTN-competitive inhibition. With a K_m for GTN of 8.7 μM and assuming competitive inhibition, the best fits gave K_i values of 16.3 ± 1.7 and 17.7 ± 1.4 μM daidzin at 10 and 100 μM GTN, respectively. The corre-

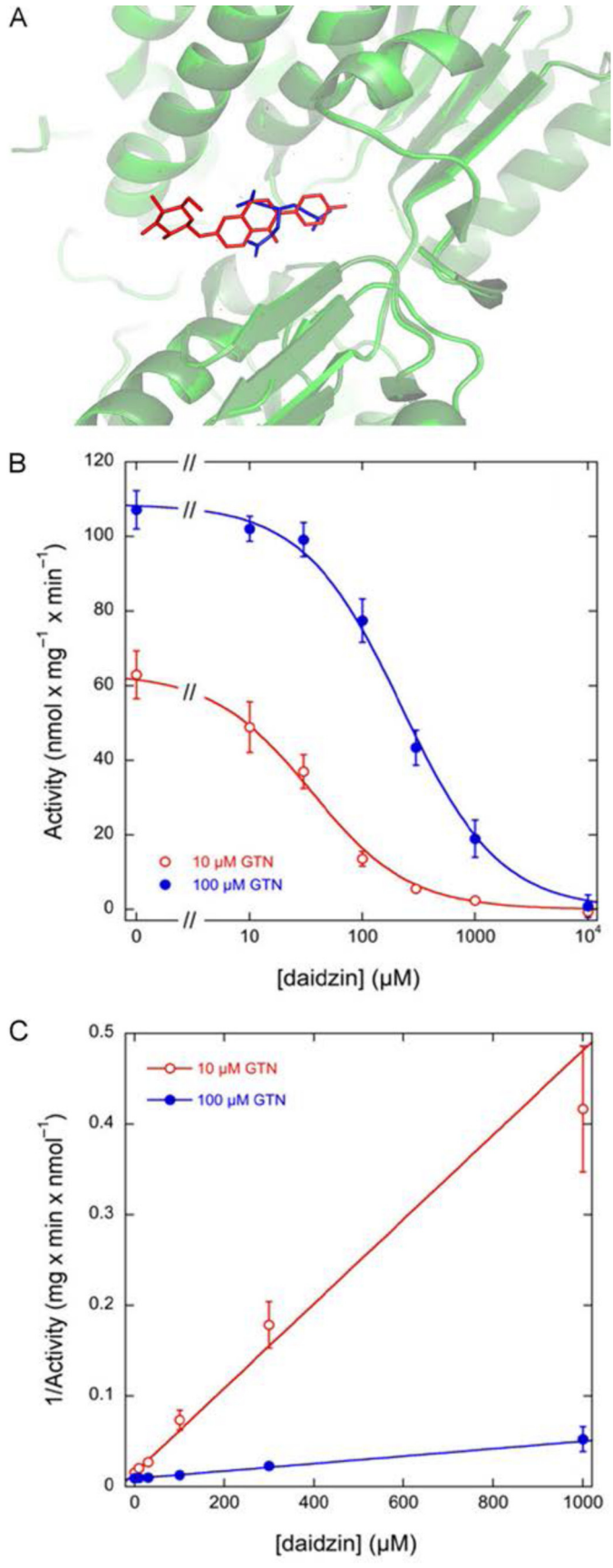

FIGURE 5. **Effect of daidzin on the denitration activity of ALDH2.** *A*, schematic representation of the GTN complexed triple mutant (*light green*) superimposed onto the daidzin bound wild-type enzyme (*dark green*) (PDB 2vle). GTN and daidzin are shown as *sticks* in *blue* and *red*, respectively. *B*, the activity of GTN denitration (10 and 100 μM GTN) was determined for varying daidzin concentrations (10 μM to 10 mM). Data are mean ± S.E. of three independent experiments. A best fit of both curves to a model assuming competitive inhibition was obtained with a K_d for GTN of 8.7 μM. *C*, corresponding Dixon plots.

sponding V_{max} values were 119 ± 3 and 118 ± 2 nmol of 1,2-GDN × min^{-1} × mg^{-1}. The value of 8.7 μM for the K_m of GTN is in excellent agreement with the value of 7 μM determined by us previously (56). The corresponding Dixon plots (Fig. 5*C*) also clearly indicated competition between GTN and daidzin with values for K_i and V_{max} of 15.0 μM and 116.3 nmol of 1,2-GDN × min^{-1} × mg^{-1}, respectively.

DISCUSSION

Subsequent to the identification of ALDH2 as the key enzyme of vascular GTN bioactivation (13) substantial work has been done to clarify the mechanism of the ALDH2/GTN reaction (14–16, 38, 56–58). Site-directed mutagenesis studies confirmed the assumption that GTN reacts with the active site Cys-302 (15). However, the exact binding mode of GTN has so far been elusive.

Therefore, we tried to determine the x-ray crystal structure of the ALDH2-GTN complex by soaking enzyme crystals with GTN. As initial attempts with crystals of the wild-type enzyme were not successful, we chose the triple mutant E268Q/C310S/C303S for further experiments. This mutant was a promising alternative, because the crystals were bigger and more robust compared with those of the wild-type. Moreover, it has a lower activity and is more slowly inactivated (16), making it a better candidate for soaking experiments.

Indeed, soaking crystals of the triple mutant gave a structure with a residual density in the active site that could best be explained by a bound GTN molecule. This interpretation is supported by the fact that GTN denitration is competitively inhibited by daidzin, which itself has been shown crystallographically to bind to the active site of ALDH2 (20).

The K_i value of daidzin for GTN denitration of 17 μM determined in the present study is much higher than for acetaldehyde dehydrogenation (0.29 μM at pH 7.5, Ref. 55). This observation is reminiscent of previous reports on the inhibition of dehydrogenation by esterase substrates and vice versa (59, 60), on the inhibition of GTN denitration by acetaldehyde (13), and on the inhibition of dehydrogenation and esterase activities by GTN (56), which also yielded much higher K_i values than expected. In line with previous suggestions (56), we propose that the phenomenon is due to imperfect overlap between the respective binding sites.

Binding of GTN to the Active Site—The structure of the active site of the ALDH2 triple mutant is virtually identical to that of the wild-type enzyme (Fig. 2*B*). This supports the assumption that its altered activity profile was truly due to the different chemical properties of the mutated residues and not due to structural perturbations of the catalytic pocket.

GTN is bound to the enzyme by hydrogen bonds of the two terminal nitrate groups and by van der Waals interactions with hydrophobic residues of the active site (Fig. 2*A*). Most remarkably, one oxygen atom of the *pro*-S nitrate group is bound to the

oxyanion hole in a manner similar to what has been proposed for aldehydes (41). The second oxygen atom is hydrogen-bonded to the side chain of Gln-268. In this way the nitrogen of the *pro*-S nitrate group of GTN is held in a position ideal for nucleophilic attack of Cys-302 leading to thionitrate formation and release of 1,2-GDN.

As in the present structure, the side chain of Cys-302 is sometimes observed in two different conformations in ALDH2 structures denoted as the resting and the attacking conformation (47). In the resting conformation, the SH-group of Cys-302 is too far away from the substrate to be catalytically competent, whereas in the attacking conformation it is in the right position to perform the nucleophilic attack on the *pro*-S nitrate group of GTN.

In the investigated mutant the two cysteines flanking the catalytically competent Cys-302 were replaced by serines. These mutations influence the catalytic activity of ALDH2 (16); inspection of the model, however, suggests that they do not change the binding mode of GTN. Ser-301 forms hydrogen bonds to the *pro*-R nitrate group of GTN, which could also be accomplished by Cys-301. Ser-303 (and by analogy Cys-303) is not directly involved in the binding of GTN at all.

In the structure of the triple mutant Gln-268 was only observed in the inside conformation. Its interaction with the *pro*-S nitrate group of GTN is only possible if the carboxamide group is in the right orientation. Without a substrate in the active site, the NH_2-group of Gln-268 maintains a hydrogen bond with the main chain carbonyl oxygen of Leu-269. However, if GTN is bound, an oxygen atom of the *pro*-S nitrate group is in close proximity to the side chain carboxamide of Gln-268, requiring a flip of this residue to establish a hydrogen bond.

In the wild-type enzyme the equivalent interaction with Glu-268 would only be possible, if the side chain of this residue were protonated. There are no clear reports in the literature regarding the protonation state of Glu-268 (in the inside conformation) except for calculations indicating an increased pK_a value (~7.6) of this residue (41). A recent study from our lab has also shown that the exchange of Glu-268 by glutamine does not significantly influence the denitration activity of the enzyme (in the absence of NAD^+) (15). We thus conclude that the binding mode of GTN, which we observe in the structure of the triple mutant should at least closely resemble binding of GTN to wild-type ALDH2.

1,2-GDN Formation—According to the current view (4, 61) the first step of ALDH2-catalyzed denitration is the nucleophilic attack of Cys-302 on one terminal nitrogen of GTN, resulting in a thionitrate adduct and release of 1,2-GDN (Scheme 1). Whereas nonenzymatic reactions produce roughly stoichiometric amounts of 1,2-GDN and 1,3-GDN (4), the specific formation of 1,2-GDN is a characteristic feature of the enzymatic bioactivation of GTN (13, 62, 63). We placed GTN in two different conformations into the density so that the resulting product would either be 1,2-GDN or 1,3-GDN. Inspection of the density strongly argued for a binding mode of GTN that yields 1,2-GDN (supplemental Fig. S2).

Although 1,2-GDN is a chiral molecule, to the best of our knowledge there are no reports in the literature showing the reaction to be stereoselective. The stereochemical outcome of the reaction depends on whether the *pro*-S or *pro*-R nitrate group interacts with Cys-302. We checked both binding modes against the experimental electron density and found one of them to fit the density slightly better (Fig. 2*A*). Our structure would thus predict the formation of the *R*-enantiomer of 1,2-GDN. However, the difference between the two binding modes was not big enough to rule out at least partial formation of the *S*-enantiomer.

Implications for the Development of New Organic Nitrates—There has been substantial debate on the properties an organic nitrate should have to be a substrate for ALDH2 (64–67). A physicochemical parameter that takes into account the propensity for two oxygen atoms in a molecule to be situated 5.8 Å apart from one another was proposed by Tzeng and Fung (68) to reliably predict the pharmacological activity of organic nitrates. This proposal is consistent with our structure, in which two oxygen atoms from each of the terminal nitrate groups are hydrogen-bonded to the enzyme and are 5.3 Å apart from each other (Fig. 2*A*). Thus we conclude that to be a good substrate for ALDH2, an organic nitrate should not only be lipophilic enough to maintain van der Waals contacts with hydrophobic residues of the catalytic pocket but should also have a polar region that can bind to residue 301.

Modifications of ALDH2 Caused by GTN—Although the production of 1,2-GDN has been confirmed experimentally (13, 38), the thionitrate intermediate has so far eluded direct observation.

The residual density of the soaked WT structure indicates a modification at the sulfur atom of Cys-302 that is trigonal planar with three additional atoms. The thionitrate that is expected to be formed in the reaction with GTN seems to be the only reasonable candidate for this species (Scheme 1).

A superposition of the structures of the soaked wild-type with that of the triple mutant revealed that the thionitrate adduct occupies the same space as the terminal nitrate group of GTN (Fig. 6). Especially, the position of the nitrogen atom and of one of the oxygen atoms (bound to the oxyanion hole) is preserved. A slight rotation of the nitro group in the intermediate precludes polar contacts with Glu-268, the side chain of which flips from the inside to the intermediate conformation. We propose that our two structures represent snapshots along the first step of GTN denitration.

The existence of the thionitrate intermediate is supported by the mass spectrometry results. The peak corresponding to the thionitrate (or sulfenyl nitrite, respectively) is more pronounced in the triple mutant, whereas it is only a small fraction in the wild-type.

In line with kinetic experiments (16), these data indicate that after 10 min of incubation with GTN under nonreducing conditions, the WT has undergone one turnover and the two main species found are the reversibly and irreversibly inhibited enzyme. In contrast, the activity of the triple mutant was strongly reduced, which is reflected by the presence of the thionitrate intermediate.

Paradoxically, when the crystals of the WT and the triple mutant were soaked with GTN, the thionitrate was only observed in the structure of the WT enzyme. Although crystal-

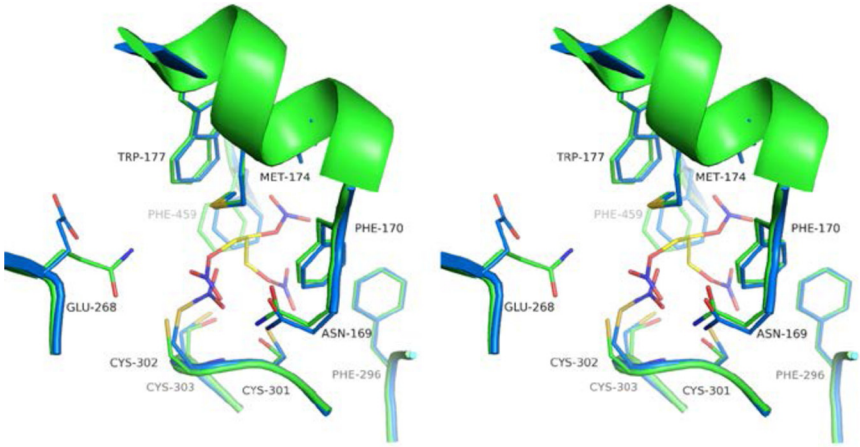

FIGURE 6. **Stereoscopic representation of the superposition of the triple mutant GTN complexed (*green*) and the WT thionitrate intermediate (*blue*) ALDH2 structures.** Active site residues as well as GTN and the thionitrate are shown as *sticks*. GTN is colored *yellow*. Alternate conformations of Cys-301 and Cys-302 are not shown. Labels refer to the wild-type.

lographic studies are unsuited for kinetic observations, some inferences about the relative stabilities of intermediates can be made on the basis of the present results. Because we grew our crystals in the presence of TCEP (which is an effective re-activator of oxidized ALDH2 (61)), the enzyme was probably capable of multiple catalytic turnover upon soaking with GTN. Under such conditions the state immediately before the slowest step in the cycle will accumulate. For the wild-type enzyme this suggests that the reaction of the thionitrate intermediate (release of nitrite, formation of a disulfide bond) is slowest under the crystallization conditions.

The situation appears to be quite different for the triple mutant. On the basis of Scheme 1, one might perhaps have expected even stronger accumulation of the thionitrate, because the main reaction pathway of the WT is blocked. The fact that we did not observe a thionitrate intermediate implies that its formation is much slower in the triple mutant. This may be explained by a strongly diminished acidity of Cys-302 in the absence of the two neighboring cysteines. The results therefore suggest that a major role of Cys-301 and Cys-303 in GTN catabolism is the stimulation of thionitrate formation.

The different behavior in the mass spectrometric experiments may be explained by the absence of a thiol regenerating compound. Consequently, the WT enzyme ends up as a 2:1 mixture of disulfide and sulfinic acid, which probably reflects the relative rates of steps *a* and *b* in Scheme 1. In the triple mutant both pathways are blocked and the thionitrate accumulated on the time scale of the experiment, although the cyclic sulfenamide and the sulfinic acid species still constituted the majority of the observed products.

Implications for the Reaction Mechanism—Our MS data of the WT support the original hypothesis of Chen *et al.* (13) that disulfide bond formation is the last step of the ADLH2/GTN reaction under nonreducing conditions (Scheme 1). However, because a similar shift is observed in the triple mutant, it is conceivable that sulfenic acid is formed during catalysis which, in the case of the mutant, undergoes cyclization to an intramolecular sulfenamide. The sulfenic acid would be generated by the attack of the thionitrate by an activated water molecule as has been proposed by Chen *et al.* (61). Indeed, in our structure of the WT-thionitrate complex, an ordered water molecule is situated between Glu-268 and Cys-302, which could fulfill this role (Fig. 3).

Based on our results we cannot discern whether sulfenic acid formation is a peculiarity of the triple mutant or if it also occurs in the WT. If a sulfenic acid is formed in the WT reaction, it may be rapidly attacked by one of the two flanking cysteine residues to form a disulfide bond because sulfenic acids are known to be quite reactive with thiol groups (69). The demonstration of sulfinic acid formation in the WT reaction (Fig. 4) strengthens the hypothesis by Wenzl *et al.* (16) that irreversible ALDH inhibition is caused by sulfenyl nitrite rearrangement followed by Glu-268-mediated oxidation (Scheme 1).

Summary—Taken together our results give insight into the different reaction steps of ALDH2 catalyzed GTN denitration, revealed the binding mode of GTN, and confirmed thionitrate as the central intermediate. Reversibly and irreversibly inhibited ALDH2 were identified by mass spectrometry as enzyme species with a disulfide or a sulfinic acid in the active site, respectively. Finally, we obtained circumstantial evidence for sulfenic acid as an intermediate in the denitration reaction. Additional studies will be required to corroborate the latter observations.

Acknowledgments—We thank Jiang Qian for assistance with MS data collection and analysis as well as the beamline staff at the European Synchrotron Radiation Facility (ESRF) in Grenoble, France, and the Deutsches Elektronensynchrotron (DESY) in Hamburg, Germany, for support during diffraction data collection.

REFERENCES

1. Marsh, N., and Marsh, A. (2000) A short history of nitroglycerine and nitric oxide in pharmacology and physiology. *Clin. Exp. Pharmacol. Physiol.* **27,** 313–319
2. Fung, H. L. (2004) Biochemical mechanism of nitroglycerin action and tolerance. Is this old mystery solved? *Annu. Rev. Pharmacol. Toxicol.* **44,** 67–85
3. Ahlner, J., Andersson, R. G., Torfgård, K., and Axelsson, K. L. (1991) Organic nitrate esters. Clinical use and mechanisms of actions. *Pharmacol. Rev.* **43,** 351–423
4. Mayer, B., and Beretta, M. (2008) The enigma of nitroglycerin bioactiva-

tion and nitrate tolerance. News, views, and troubles. *Br. J. Pharmacol.* **155,** 170–184
5. Racker, E. (1949) Aldehyde dehydrogenase, a diphosphopyridine nucleotide-linked enzyme. *J. Biol. Chem.* **177,** 883–892
6. Yoshida, A., Rzhetsky, A., Hsu, L. C., and Chang, C. (1998) Human aldehyde dehydrogenase gene family. *Eur. J. Biochem.* **251,** 549–557
7. Marchitti, S. A., Brocker, C., Stagos, D., and Vasiliou, V. (2008) Non-P450 aldehyde oxidizing enzymes. The aldehyde dehydrogenase superfamily. *Expert Opin. Drug Met. Toxicol*. **4,** 697–720
8. Klyosov, A. A., Rashkovetsky, L. G., Tahir, M. K., and Keung, W. M. (1996) Possible role of liver cytosolic and mitochondrial aldehyde dehydrogenases in acetaldehyde metabolism. *Biochemistry* **35,** 4445–4456
9. Goedde, H. W., Agarwal, D. P., Fritze, G., Meier-Tackmann, D., Singh, S., Beckmann, G., Bhatia, K., Chen, L. Z., Fang, B., and Lisker, R. (1992) Distribution of ADH2 and ALDH2 genotypes in different populations. *Hum. Genet.* **88,** 344–346
10. Muto, M., Hitomi, Y., Ohtsu, A., Ebihara, S., Yoshida, S., and Esumi, H. (2000) Association of aldehyde dehydrogenase 2 gene polymorphism with multiple oesophageal dysplasia in head and neck cancer patients. *Gut* **47,** 256–261
11. Yokoyama, A., Muramatsu, T., Omori, T., Matsushita, S., Yoshimizu, H., Higuchi, S., Yokoyama, T., Maruyama, K., and Ishii, H. (1999) Alcohol and aldehyde dehydrogenase gene polymorphisms influence susceptibility to esophageal cancer in Japanese alcoholics. *Alcohol Clin. Exp. Res.* **23,** 1705–1710
12. Feldman, R. I., and Weiner, H. (1972) Horse liver aldehyde dehydrogenase. II. Kinetics and mechanistic implications of the dehydrogenase and esterase activity. *J. Biol. Chem.* **247,** 267–272
13. Chen, Z., Zhang, J., and Stamler, J. S. (2002) Identification of the enzymatic mechanism of nitroglycerin bioactivation. *Proc. Natl. Acad. Sci. U.S.A.* **99,** 8306–8311
14. Beretta, M., Gruber, K., Kollau, A., Russwurm, M., Koesling, D., Goessler, W., Keung, W. M., Schmidt, K., and Mayer, B. (2008) Bioactivation of nitroglycerin by purified mitochondrial and cytosolic aldehyde dehydrogenases. *J. Biol. Chem.* **283,** 17873–17880
15. Wenzl, M. V., Beretta, M., Gorren, A. C., Zeller, A., Baral, P. K., Gruber, K., Russwurm, M., Koesling, D., Schmidt, K., and Mayer, B. (2009) Role of the general base Glu-268 in nitroglycerin bioactivation and superoxide formation by aldehyde dehydrogenase-2. *J. Biol. Chem.* **284,** 19878–19886
16. Wenzl, M. V., Beretta, M., Griesberger, M., Russwurm, M., Koesling, D., Schmidt, K., Mayer, B., and Gorren, A. C. (2011) Site-directed mutagenesis of aldehyde dehydrogenase-2 suggests three distinct pathways of nitroglycerin biotransformation. *Mol. Pharmacol.* **80,** 258–266
17. Münzel, T., Daiber, A., and Mülsch, A. (2005) Explaining the phenomenon of nitrate tolerance. *Circ. Res.* **97,** 618–628
18. Zheng, C. F., Wang, T. T., and Weiner, H. (1993) Cloning and expression of the full-length cDNAS encoding human liver class 1 and class 2 aldehyde dehydrogenase. *Alcohol. Clin. Exp. Res.* **17,** 828–831
19. Perez-Miller, S., Younus, H., Vanam, R., Chen, C. H., Mochly-Rosen, D., and Hurley, T. D. (2010) Alda-1 is an agonist and chemical chaperone for the common human aldehyde dehydrogenase 2 variant. *Nat. Struct. Mol. Biol.* **17,** 159–164
20. Lowe, E. D., Gao, G. Y., Johnson, L. N., and Keung, W. M. (2008) Structure of daidzin, a naturally occurring anti-alcohol addiction agent, in complex with human mitochondrial aldehyde dehydrogenase. *J. Med. Chem.* **51,** 4482–4487
21. Larson, H. N., Zhou, J., Chen, Z., Stamler, J. S., Weiner, H., and Hurley, T. D. (2007) Structural and functional consequences of coenzyme binding to the inactive asian variant of mitochondrial aldehyde dehydrogenase. Roles of residues 475 and 487. *J. Biol. Chem.* **282,** 12940–12950
22. Perez-Miller, S. J., and Hurley, T. D. (2003) Coenzyme isomerization is integral to catalysis in aldehyde dehydrogenase. *Biochemistry* **42,** 7100–7109
23. Hurley, T. D., Perez-Miller, S., and Breen, H. (2001) Order and disorder in mitochondrial aldehyde dehydrogenase. *Chem.-Biol. Interact.* **130,** 3–14
24. Ni, L., Zhou, J., Hurley, T. D., and Weiner, H. (1999) Human liver mitochondrial aldehyde dehydrogenase. Three-dimensional structure and the restoration of solubility and activity of chimeric forms. *Protein Sci.* **8,** 2784–2790
25. Steinmetz, C. G., Xie, P., Weiner, H., and Hurley, T. D. (1997) Structure of mitochondrial aldehyde dehydrogenase. The genetic component of ethanol aversion. *Structure* **5,** 701–711
26. Feldman, R. I., and Weiner, H. (1972) Horse liver aldehyde dehydrogenase. I. Purification and characterization. *J. Biol. Chem.* **247,** 260–266
27. McCarthy, A. A., Brockhauser, S., Nurizzo, D., Theveneau, P., Mairs, T., Spruce, D., Guijarro, M., Lesourd, M., Ravelli, R. B., and McSweeney, S. (2009) A decade of user operation on the macromolecular crystallography MAD beamline ID14–4 at the ESRF. *J. Synchrotron Radiat.* **16,** 803–812
28. Kabsch, W. (2010) XDS. *Acta Crystallogr. D Biol. Crystallogr.* **66,** 125–132
29. Evans, P. (2006) Scaling and assessment of data quality. *Acta Crystallogr. D Biol. Crystallogr.* **62,** 72–82
30. Adams, P. D., Afonine, P. V., Bunkoczi, G., Chen, V. B., Davis, I. W., Echols, N., Headd, J. J., Hung, L. W., Kapral, G. J., Grosse-Kunstleve, R. W., McCoy, A. J., Moriarty, N. W., Oeffner, R., Read, R. J., Richardson, D. C., Richardson, J. S., Terwilliger, T. C., and Zwart, P. H. (2010) PHENIX. A comprehensive Python-based system for macromolecular structure solution. *Acta Crystallogr. D Biol. Crystallogr.* **66,** 213–221
31. McCoy, A. J., Grosse-Kunstleve, R. W., Adams, P. D., Winn, M. D., Storoni, L. C., and Read, R. J. (2007) Phaser crystallographic software. *J. Appl. Crystallogr.* **40,** 658–674
32. Emsley, P., Lohkamp, B., Scott, W. G., and Cowtan, K. (2010) Features and development of Coot. *Acta Crystallogr. D Biol. Crystallogr.* **66,** 486–501
33. Terwilliger, T. C., Adams, P. D., Moriarty, N. W., and Cohn, J. D. (2007) Ligand identification using electron-density map correlations. *Acta Crystallogr. D Biol. Crystallogr.* **63,** 101–107
34. Terwilliger, T. C., Klei, H., Adams, P. D., Moriarty, N. W., and Cohn, J. D. (2006) Automated ligand fitting by core-fragment fitting and extension into density. *Acta Crystallogr. D Biol. Crystallogr.* **62,** 915–922
35. Schüttelkopf, A. W., and van Aalten, D. M. (2004) PRODRG. A tool for high-throughput crystallography of protein-ligand complexes. *Acta Crystallogr. D Biol. Crystallogr.* **60,** 1355–1363
36. Espenbetov, A. A., Antipin, M. Y., Struchkov, Y. T., Philippov, V. A., Tsirelson, V. G., Ozerov, R. P., and Svetlov, B. S. (1984) Structure of 1,2,3-propanetriol trinitrate (β-modification), C3h5n3o9. *Acta Crystallogr. Sect. C Cryst. Struct. Commun.* **40,** 2096–2098
37. Goto, K., Hino, Y., Kawashima, T., Kaminaga, M., Yano, E., Yamamoto, G., Takagi, N., and Nagase, S. (2000) Synthesis and crystal structure of a stable *S*-nitrosothiol bearing a novel steric protection group and of the corresponding *S*-nitrothiol. *Tetrahedron Lett.* **41,** 8479–8483
38. Kollau, A., Hofer, A., Russwurm, M., Koesling, D., Keung, W. M., Schmidt, K., Brunner, F., and Mayer, B. (2005) Contribution of aldehyde dehydrogenase to mitochondrial bioactivation of nitroglycerin. Evidence for the activation of purified soluble guanylate cyclase through direct formation of nitric oxide. *Biochem. J.* **385,** 769–777
39. Liu, Z. J., Sun, Y. J., Rose, J., Chung, Y. J., Hsiao, C. D., Chang, W. R., Kuo, I., Perozich, J., Lindahl, R., Hempel, J., and Wang, B. C. (1997) The first structure of an aldehyde dehydrogenase reveals novel interactions between NAD and the Rossmann-fold. *Nat. Struct. Biol.* **4,** 317–326
40. Hammen, P. K., Allali-Hassani, A., Hallenga, K., Hurley, T. D., and Weiner, H. (2002) Multiple conformations of NAD and NADH when bound to human cytosolic and mitochondrial aldehyde dehydrogenase. *Biochemistry* **41,** 7156–7168
41. Muñoz-Clares, R. A., González-Segura, L., and Díaz-Sánchez, A. G. (2011) Crystallographic evidence for active-site dynamics in the hydrolytic aldehyde dehydrogenases. Implications for the deacylation step of the catalyzed reaction. *Chem.-Biol. Interact.* **191,** 137–146
42. Cobessi, D., Tête-Favier, F., Marchal, S., Azza, S., Branlant, G., and Aubry, A. (1999) Apo and holo crystal structures of an NADP-dependent aldehyde dehydrogenase from Streptococcus mutans. *J. Mol. Biol.* **290,** 161–173
43. Tsybovsky, Y., Donato, H., Krupenko, N. I., Davies, C., and Krupenko, S. A. (2007) Crystal structures of the carboxyl-terminal domain of rat 10-formyltetrahydrofolate dehydrogenase. Implications for the catalytic mechanism of aldehyde dehydrogenases. *Biochemistry* **46,** 2917–2929
44. D'Ambrosio, K., Pailot, A., Talfournier, F., Didierjean, C., Benedetti, E., Aubry, A., Branlant, G., and Corbier, C. (2006) The first crystal structure

of a thioacylenzyme intermediate in the ALDH family. New coenzyme conformation and relevance to catalysis. *Biochemistry* **45,** 2978–2986
45. Gruez, A., Roig-Zamboni, V., Grisel, S., Salomoni, A., Valencia, C., Campanacci, V., Tegoni, M., and Cambillau, C. (2004) Crystal structure and kinetics identify *Escherichia coli YdcW* gene product as a medium chain aldehyde dehydrogenase. *J. Mol. Biol.* **343,** 29–41
46. Inagaki, E., Ohshima, N., Takahashi, H., Kuroishi, C., Yokoyama, S., and Tahirov, T. H. (2006) Crystal structure of *Thermus thermophilus* δ1-pyrroline-5-carboxylate dehydrogenase. *J. Mol. Biol.* **362,** 490–501
47. González-Segura, L., Rudiño-Piñera, E., Muñoz-Clares, R. A., and Horjales, E. (2009) The crystal structure of a ternary complex of betaine aldehyde dehydrogenase from *Pseudomonas aeruginosa* provides new insight into the reaction mechanism and shows a novel binding mode of the 2′-phosphate of $NADP^+$ and a novel cation binding site. *J. Mol. Biol.* **385,** 542–557
48. Larson, H. N., Weiner, H., and Hurley, T. D. (2005) Disruption of the coenzyme binding site and dimer interface revealed in the crystal structure of mitochondrial aldehyde dehydrogenase "Asian" variant. *J. Biol. Chem.* **280,** 30550–30556
49. Muñoz-Clares, R. A., Díaz-Sánchez, A. G., González-Segura, L., and Montiel, C. (2010) Kinetic and structural features of betaine aldehyde dehydrogenases. Mechanistic and regulatory implications. *Arch. Biochem. Biophys.* **493,** 71–81
50. Lorentzen, E., Hensel, R., Knura, T., Ahmed, H., and Pohl, E. (2004) Structural basis of allosteric regulation and substrate specificity of the nonphosphorylating glyceraldehyde-3-phosphate dehydrogenase from *Thermoproteus tenax*. *J. Mol. Biol.* **341,** 815–828
51. Li, Z., Sau, A. K., Furdui, C. M., and Anderson, K. S. (2005) Probing the role of tightly bound phosphoenolpyruvate in *Escherichia coli* 3-deoxy-D-manno-octulosonate-8-phosphate synthase catalysis using quantitative time-resolved electrospray ionization mass spectrometry in the millisecond time range. *Anal. Biochem.* **343,** 35–47
52. Yang, J., Groen, A., Lemeer, S., Jans, A., Slijper, M., Roe, S. M., den Hertog, J., and Barford, D. (2007) Reversible oxidation of the membrane distal domain of receptor PTPα is mediated by a cyclic sulfenamide. *Biochemistry* **46,** 709–719
53. Salmeen, A., Andersen, J. N., Myers, M. P., Meng, T. C., Hinks, J. A., Tonks, N. K., and Barford, D. (2003) Redox regulation of protein tyrosine phosphatase 1B involves a sulphenyl-amide intermediate. *Nature* **423,** 769–773
54. van Montfort, R. L., Congreve, M., Tisi, D., Carr, R., and Jhoti, H. (2003) Oxidation state of the active-site cysteine in protein-tyrosine phosphatase 1B. *Nature* **423,** 773–777
55. Keung, W. M., Klyosov, A. A., and Vallee, B. L. (1997) Daidzin inhibits mitochondrial aldehyde dehydrogenase and suppresses ethanol intake of Syrian golden hamsters. *Proc. Natl. Acad. Sci. U.S.A.* **94,** 1675–1679
56. Beretta, M., Sottler, A., Schmidt, K., Mayer, B., and Gorren, A. C. (2008) Partially irreversible inactivation of mitochondrial aldehyde dehydrogenase by nitroglycerin. *J. Biol. Chem.* **283,** 30735–30744
57. Beretta, M., Gorren, A. C., Wenzl, M. V., Weis, R., Russwurm, M., Koesling, D., Schmidt, K., and Mayer, B. (2010) Characterization of the East Asian variant of aldehyde dehydrogenase-2 bioactivation of nitroglycerin and effects of Alda-1. *J. Biol. Chem.* **285,** 943–952
58. Beretta, M., Wölkart, G., Schernthaner, M., Griesberger, M., Neubauer, R., Schmidt, K., Sacherer, M., Heinzel, F. R., Kohlwein, S. D., and Mayer, B. (2012) Vascular bioactivation of nitroglycerin is catalyzed by cytosolic aldehyde dehydrogenase-2. *Circ. Res.* **110,** 385–393
59. Mukerjee, N., and Pietruszko, R. (1992) Human mitochondrial aldehyde dehydrogenase substrate specificity. Comparison of esterase with dehydrogenase reaction. *Arch. Biochem. Biophys.* **299,** 23–29
60. Tu, G. C., and Weiner, H. (1988) Evidence for two distinct active sites on aldehyde dehydrogenase. *J. Biol. Chem.* **263,** 1218–1222
61. Chen, Z., and Stamler, J. S. (2006) Bioactivation of nitroglycerin by the mitochondrial aldehyde dehydrogenase. *Trends Cardiovasc. Med.* **16,** 259–265
62. Brien, J. F., McLaughlin, B. E., Breedon, T. H., Bennett, B. M., Nakatsu, K., and Marks, G. S. (1986) Biotransformation of glyceryl trinitrate occurs concurrently with relaxation of rabbit aorta. *J. Pharmacol. Exp. Ther.* **237,** 608–614
63. Sage, P. R., de la Lande, I. S., Stafford, I., Bennett, C. L., Phillipov, G., Stubberfield, J., and Horowitz, J. D. (2000) Nitroglycerin tolerance in human vessels. Evidence for impaired nitroglycerin bioconversion. *Circulation* **102,** 2810–2815
64. Wessler, C., Homann, A., Fricke, U., and Lehmann, J. (2003) NO donors, part 8 (1). Synthesis and vasodilating activities of substituted benzylnitrates compared to cyclohexylmethylnitrate and GTN. *Eur. J. Med. Chem.* **38,** 581–586
65. Chegaev, K., Lazzarato, L., Marcarino, P., Di Stilo, A., Fruttero, R., Vanthuyne, N., Roussel, C., and Gasco, A. (2009) Synthesis of some novel organic nitrates and comparative *in vitro* study of their vasodilator profile. *J. Med. Chem.* **52,** 4020–4025
66. Koenig, A., Roegler, C., Lange, K., Daiber, A., Glusa, E., and Lehmann, J. (2007) NO donors. Part 16, investigations on structure-activity relationships of organic mononitrates reveal 2-nitrooxyethyl ammonium nitrate as a high potent vasodilator. *Bioorg. Med. Chem. Lett.* **17,** 5881–5885
67. Wenzel, P., Hink, U., Oelze, M., Seeling, A., Isse, T., Bruns, K., Steinhoff, L., Brandt, M., Kleschyov, A. L., Schulz, E., Lange, K., Weiner, H., Lehmann, J., Lackner, K. J., Kawamoto, T., Münzel, T., and Daiber, A. (2007) Number of nitrate groups determines reactivity and potency of organic nitrates. A proof of concept study in ALDH-$2^{-/-}$ mice. *Br. J. Pharmacol.* **150,** 526–533
68. Tzeng, T. B., and Fung, H. L. (1992) Structure activity relationship of organic nitrates. An exploratory hypothesis via molecular models. *Med. Hypotheses* **37,** 58–62
69. Poole, L. B., Karplus, P. A., and Claiborne, A. (2004) Protein sulfenic acids in redox signaling. *Annu. Rev. Pharmacol. Toxicol.* **44,** 325–347